Journal of Applied Physics

Thickness-dependent thermoelectric properties of $Si_{1-x}Ge_x$ films formed by Al-induced layer exchange

Cite as: J. Appl. Phys. **129**, 015303 (2021); https://doi.org/10.1063/5.0025099
Submitted: 13 August 2020 • Accepted: 10 December 2020 • Published Online: 04 January 2021

T. Ozawa, K. Kusano, M. Murata, et al.

Journal of Applied Physics ARTICLE scitation.org/journal/jap

Thickness-dependent thermoelectric properties of $Si_{1-x}Ge_x$ films formed by Al-induced layer exchange

Cite as: J. Appl. Phys. **129**, 015303 (2021); doi: 10.1063/5.0025099
Submitted: 13 August 2020 · Accepted: 10 December 2020 ·
Published Online: 4 January 2021

View Online Export Citation CrossMark

T. Ozawa,[1] K. Kusano,[1] M. Murata,[2,a)] A. Yamamoto,[2] T. Suemasu,[1] and K. Toko[1,3,a)]

AFFILIATIONS

[1]Institute of Applied Physics, University of Tsukuba, 1-1-1 Tennodai, Tsukuba, Ibaraki 305-8573, Japan
[2]Research Institute for Energy Conservation, AIST, Tsukuba, Ibaraki 305-8569, Japan
[3]PRESTO, Japan Science and Technology Agency, 4-1-8 Honcho, Kawaguchi, Saitama 332-0012, Japan

[a)]**Authors to whom correspondence should be addressed:** m.murata@aist.go.jp and toko@bk.tsukuba.ac.jp

ABSTRACT

Highly reliable, thin-film thermoelectric generators are strongly desired for future sensor advancements. Al-induced layer exchange is a unique method for producing thermoelectric SiGe layers on a flexible plastic substrate at low temperatures. In this study, we investigated the thickening of the $Si_{1-x}Ge_x$ ($x = 0$, 0.6, and 1) layers to improve the thermoelectric output power. The upper limit of the film thickness was approximately 1000 nm, while it influenced the crystal and electrical properties of the resulting $Si_{1-x}Ge_x$ layers. The $Si_{0.4}Ge_{0.6}$ layer formed at 400 °C exhibited a high power factor of up to 850 $\mu W\,m^{-1}\,K^{-2}$ at room temperature, which is the record-high value among p-type SiGe obtained at low temperature (<900 °C). The dimensionless figure of merit was determined to be 0.12 from the power factor and the thermal conductivity of 2.2 $W\,m^{-1}\,K^{-1}$. The sequential layer exchange allowed us to form a 2000-nm-thick SiGe layer. Furthermore, the output power density was almost proportional to the film thickness and reached 37 nW cm^{-2} at room temperature under a temperature difference of 10 K. These achievements will present practical applications for next-generation thin-film thermoelectric generators based on highly reliable, human-friendly materials.

I. INTRODUCTION

Research on flexible thermoelectric generators (TEGs) has significantly progressed in recent years.[1] For fabricating highly versatile flexible TEGs, the direct synthesis of thermoelectric materials on plastic substrates is the most promising approach.[2] Because plastics typically have low heat resistance, most research has focused on organic materials with low synthesis temperatures.[3] However, organic materials inherently suffer from thermal deterioration, while some applications, including healthcare, will require high reliability.

The flexible thermoelectric application of inorganic materials, such as metal compounds,[4–6] oxides,[7] and graphene,[8] has also been active. The SiGe alloy has the highest reliability among thermoelectric materials as it has been used for decades in space applications.[9–11] Additionally, Si and Ge are suitable materials for electronic devices close to humans because they are nontoxic and relatively abundant. Therefore, SiGe is a promising candidate for human-friendly wearable TEGs. Moreover, researchers have developed thermoelectric SiGe thin films using laser sintering,[12] sputtering,[13,14] chemical vapor deposition,[15–19] electrophoretic deposition,[20] solid-phase crystallization,[21,22] and metal-induced crystallization.[23] However, the formation of crystalline SiGe generally requires high temperatures (>500 °C). Furthermore, the lower temperature process makes it more difficult to activate the dopants in SiGe and, therefore, obtain high thermoelectric performance.

Metal-induced layer exchange has enabled low-temperature synthesis and high-concentration doping in crystalline SiGe thin films.[23,24] We synthesized 50-nm-thick SiGe layers at ≤400 °C over the entire composition range using layer exchange techniques.[25,26] In Al-induced layer exchange (ALILE), Al has two roles: (i) a metal catalyst for layer exchange and (ii) a p-type dopant for SiGe. After the ALILE, the resulting SiGe layer contains activated Al atoms according to the solid solubility limit in a self-organizing manner.[25]

Furthermore, the B addition in ALILE results in a p-type SiGe layer exhibiting a power factor (PF) of 400 μW m^{-1} K^{-2} on glass and 240 μW m^{-1} K^{-2} on a plastic substrate.[27]

Considering that the output power of the thin-film TEG is basically proportional to the film volume, the thickness (50 nm) of the SiGe layers is too small for practical applications. Conversely, no literature has examined thick (>μm) film synthesis in layer exchange. Thus, this study investigates the upper limit of the SiGe thickness during ALILE and the influence of the thickness on the film properties and TEG performance. We update the PF of the SiGe layer to 850 μW m^{-1} K^{-2} and demonstrate that the output power increases with the film thickness.

II. EXPERIMENT

Figure 1(a) presents a schematic of the ALILE process. We prepared Al and amorphous (a-) $Si_{1-x}Ge_x$ (x: 0, 0.6, and 1) layers (thickness t: 50, 300, 500, 1000, and 2000 nm each) on a SiO_2 glass substrate at room temperature (RT) using radio frequency (RF) magnetron sputtering (a base pressure of 3.0×10^{-4} Pa) with an Ar plasma. The RF power was set to 50 W. The samples were then annealed in an N_2 atmosphere for 30 h at 450 °C (Si), 400 °C ($Si_{0.4}Ge_{0.6}$), and 350 °C (Ge). The Al layer was then etched away with an HF solution (HF 1.5%). The SiGe layers were evaluated using scanning electron microscopy (SEM) equipped with an electron backscattering diffraction (EBSD) analysis attachment. To evaluate the hole mobility μ_p and the hole concentration p, the Hall effect measurement was performed with the Van der Pauw method using the Bio-Rad HL5500PC system with a 3200 G permanent magnet. The thermoelectric measurements for the electrical conductivity σ and the Seebeck coefficient S were performed using the Advance-Riko ZEM system, where the sample was fixed to a ceramic stage using Ag paste.[25] The thermal conductivity κ was evaluated using the PicoTherm PicoTR. The output power was evaluated using a current–voltage measuring device with the indirect resistance heater and Stirling refrigerator producing an in-plane thermal gradient from the heating to the cooling region, where a differential thermocouple was mechanically contacted at the sample surface to monitor the temperature. The current and voltage were measured with Cu wires connected across the sample.

III. RESULTS AND DISCUSSION

For the samples with $t \leq 1000$ nm, the layers remaining on the substrates after the removal of Al were evaluated via Raman spectroscopy and SEM. The Raman spectra in Fig. 2(a) show the peaks corresponding to the Si–Si, Si–Ge, and Ge–Ge vibrational modes,

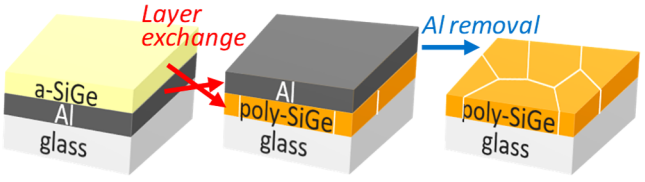

FIG. 1. Schematic of the ALILE growth of $Si_{1-x}Ge_x$.

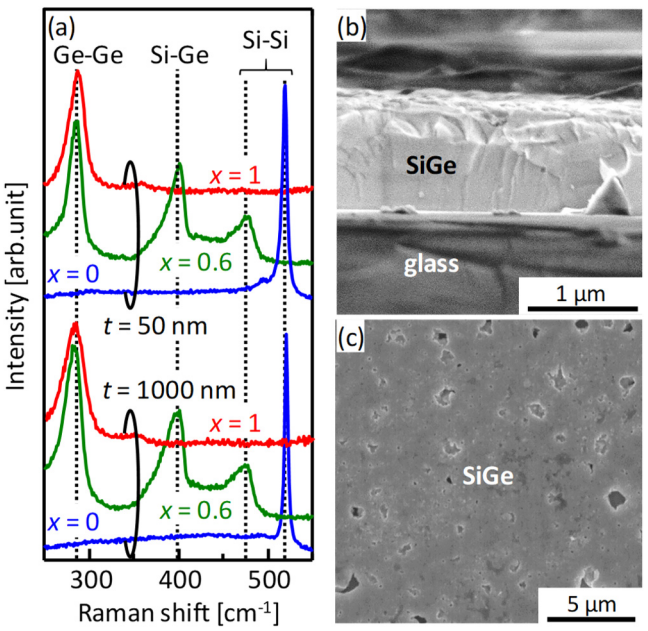

FIG. 2. Characterization of the $Si_{1-x}Ge_x$ ($x = 0$, 0.6, and 1) samples with $t = 1000$ nm after Al removal. (a) Raman spectra. (b) Cross-sectional and (c) surface SEM images.

indicating that crystalline $Si_{1-x}Ge_x$ layers form on the substrates for all samples.[28] Figure 2(b) shows that t of the resulting SiGe layer is approximately 1000 nm, as intended. Similar results were obtained for pure Si and Ge. Figure 2(c) shows that the 1000-nm-thick SiGe layer covers almost the entire surface of the substrate, though it has some voids. We note that when $t = 2000$ nm, the upper amorphous layer was crystallized before the SiGe layer reached the substrate, which inhibited the complete layer exchange. Thus, in the Al–SiGe system under the current growth condition, the upper limit of t is approximately 1000 nm.

Figure 3(a) shows the inverse pole figure (IPF) images of the samples derived from the EBSD measurements. All samples are polycrystalline where the grain size varies with t. As shown in Fig. 3(b), the Si and Ge samples with $t = 50$ nm have grains of several micrometers, which is an order of magnitude smaller than that of ALILE with a diffusion control layer.[24,25] This is an advantage of TEGs because grain boundaries scatter phonons and lower κ.[29] For Si and Ge, the grain size decreases significantly with increasing t. This behavior occurs because when the film is thicker, the crystal nucleus is easily generated at the Al grain boundary and the nucleation frequency is higher.[23] The grains of SiGe are smaller than those of Si and Ge for $t = 50$ nm, similar to the case where the diffusion control layer is provided.[25] Owing to this behavior, for SiGe, the decrease in grain size due to the increase in t is not remarkable.

All the samples exhibited p-type conduction because of the Al acceptors. Figure 4(a) shows that μ_p decreases with increasing t for Si and Ge. Considering the t dependence of the grain size (Fig. 3),

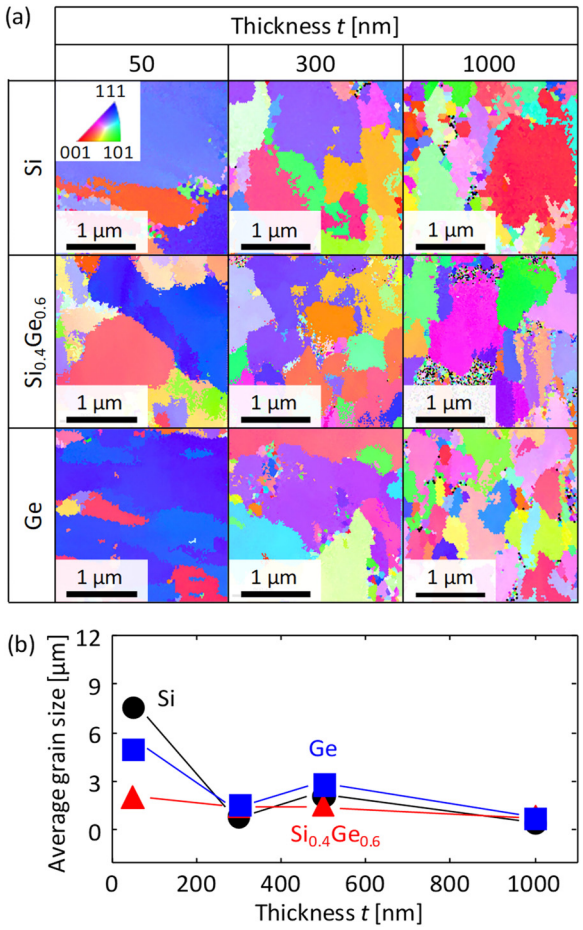

FIG. 3. Grain size of $Si_{1-x}Ge_x$ ($x = 0$, 0.6, and 1) layers analyzed by EBSD. (a) IPF images for $t = 50$, 300, and 1000 nm. The colors indicate the crystal orientation according to the color key. (b) t dependence of the average grain size quantitatively calculated from EBSD analysis software.

this behavior is likely due to grain boundary scattering commonly found in polycrystalline semiconductors.[30,31] For $Si_{0.4}Ge_{0.6}$, where the effect of t on the grain size is small (Fig. 3), μ_p increases as t increases and peaks at $t = 500$ nm. The similar behavior is common for semiconductor thin films and has been explained in terms of interfacial scattering.[31] However, according to the Drude model, the mean free path of holes in bulk single-crystal SiGe is estimated to be approximately a few tens nm due to phonon scattering alone and further reduced by impurity scattering. Considering the order of the mean free path, the large improvement in μ_p for $Si_{0.4}Ge_{0.6}$ from $t = 300$ nm to 500 nm cannot be explained only by the reduction of interfacial scattering. To fully elucidate the cause of the t dependence of μ_p in $Si_{0.4}Ge_{0.6}$, detailed and extensive research on crystallinity and SiGe composition will be essential. Figure 4(b) shows that p increases with increasing x, while it does not depend on t. This behavior is due to the ALILE feature, where p is determined by the solubility limit of Al in $Si_{1-x}Ge_x$.[24] Because the solubility limit of Al is higher in Ge than in Si,[32] p increases with x. Figure 4(c) shows that σ also increases with increasing x because σ is proportional to p. For Si and Ge, σ decreases with increasing t, reflecting a lower μ_p [Fig. 4(a)] because of the smaller grain size. In contrast, for $Si_{0.4}Ge_{0.6}$, σ peaks at $t = 500$ nm, reflecting the μ_p behavior [Fig. 4(a)]. Figure 4(d) shows that S decreases with increasing x reflecting two factors: (i) the higher x makes the effective mass of holes smaller according to the basic physical properties of $Si_{1-x}Ge_x$[9] and (ii) the higher x also makes p higher due to the higher solubility limit of Al in $Si_{1-x}Ge_x$ [Fig. 4(b)]. As with p, S does not explicitly depend on t. Figure 4(e) shows that PF has a t dependence reflecting σ. The highest PF larger than $850\,\mu W\,m^{-1}\,K^{-2}$ was obtained for $Si_{0.4}Ge_{0.6}$ with $t = 500$ nm, where μ_p and σ have a peak. This PF is the highest recorded value among p-type SiGe obtained at low temperatures (<900 °C). The cross-plane κ value of the $Si_{0.4}Ge_{0.6}$ sample with $t = 500$ nm was determined to be $2.2\,W\,m^{-1}\,K^{-1}$. The low κ value is likely owing to phonon scattering by both high-density grain boundaries due to the small grains[29] and the SiGe alloy structure.[9] From the PF and κ values, the dimensionless figure of merit is determined to be 0.12 at RT. This value is

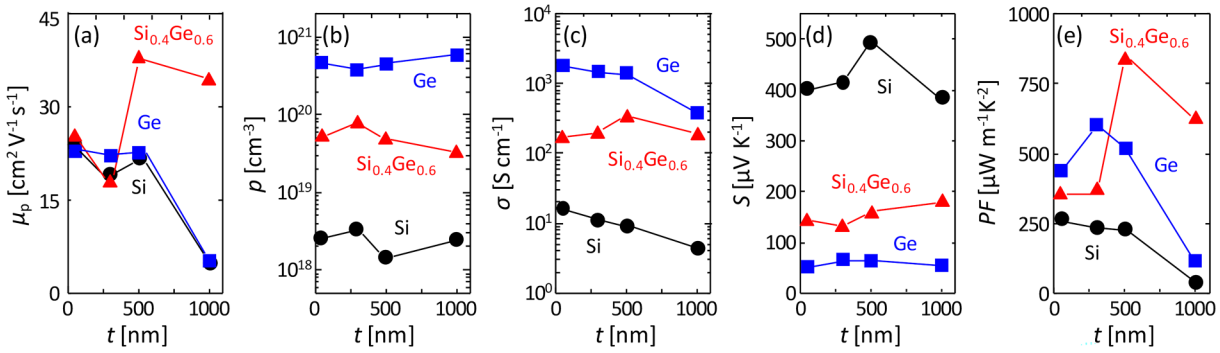

FIG. 4. Electrical and thermoelectric properties at RT for the samples as a function of the film thickness t. (a) Hole mobility μ_p. (b) Hole concentration p. (c) Electrical conductivity σ. (d) Seebeck coefficient S. (e) Power factor PF.

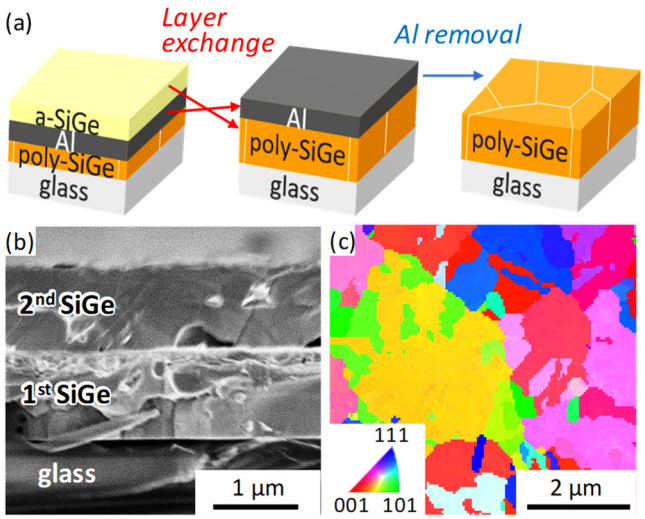

FIG. 5. (a) Schematic of the sequential layer exchange growth of $Si_{0.4}Ge_{0.6}$. (b) Cross-sectional SEM and (c) IPF image of the resulting sample after Al removal. The colors indicate the crystal orientation according to the color key.

higher than that of bulk-SiGe[9] and most p-type SiGe layers are formed at low temperature.

As described above, SiGe formed by ALILE presents a high *PF* even in thick films. However, the upper limit of the thickness is approximately 1000 nm. Therefore, we examined the sequential layer exchange that enables thicker SiGe layers, as shown in Fig. 5(a). A $Si_{0.4}Ge_{0.6}$ layer with $t = 1000$ nm was formed by the same ALILE process on a $Si_{0.4}Ge_{0.6}$ layer with $t = 1000$ nm. Figure 5(b) shows that a 2000-nm-thick SiGe layer forms on a glass substrate after Al removal by sequential layer exchange. Figure 5(c) shows that the grain size for $t = 2000$ nm is slightly larger than that for $t = 1000$ nm [Fig. 3(a)]. A similar behavior was reported in a previous study on ALILE-Si, suggesting that the upper SiGe layer is epitaxially grown by taking over some grains of the lower SiGe layer.[33] The SiGe at $t = 2000$ nm exhibited the p value of 3×10^{19} cm^{-3}, which is almost equivalent to that for $t = 1000$ nm. Thus, we have demonstrated that the sequential layer exchange of SiGe is possible, implying, in principle, that there is no limit to thickening.

Figures 6(a)–6(c) show that σ, S, and PF monotonously decrease or increase with the increasing measurement temperature, which is similar to the general thermoelectric properties of SiGe.[9] The σ value for $t = 2000$ nm is lower than that for $t = 1000$ nm, while the S values are almost the same. The SEM image in Fig. 5(b) shows that the 2000-nm-thick sample has an interlayer between the first and second ALILE-SiGe layers, which may scatter holes and reduce their mean free path. Although the PF value for $t = 2000$ nm is slightly lower than that for $t = 1000$ nm reflecting the difference in σ, it exhibits a relatively high value (500 μW m^{-1} K^{-2}) at RT. We measured the t dependence of the output power of ALILE-SiGe using the measuring setup shown in Fig. 6(d). The temperature difference between both ends of the sample was fixed at 10 K, and the sample stage was fixed at 300 K. Figure 6(e) shows that, for each t, the open-circuit voltage is almost consistent with the value calculated from S. The short-circuit current increases with increasing t, reflecting an increasing cross-sectional area due to the increasing t. The maximum output power density increases with increasing t and reaches 37 nW cm^{-2} for $t = 2000$ nm. This is a high value for environmentally friendly, inorganic thin films synthesized below the heat-resistant temperature of plastic substrates (~400 °C). This result indicates that a device with a several-cm size can output μW power, which is potentially useful for future wearable sensors.

IV. CONCLUSION

In the low-temperature ALILE, the upper limit of t was approximately 1000 nm for the entire SiGe composition range. The grain size and σ decreased with increasing t for pure Si and Ge, while they were almost constant with t for $Si_{0.4}Ge_{0.6}$. Consequently, for a large t (≥500 nm), the $Si_{0.4}Ge_{0.6}$ layer exhibited a high PF of up to 850 μW m^{-1} K^{-2}. The dimensionless figure of merit was determined to be 0.12 from the power factor and the thermal conductivity of 2.2 W m^{-1} K^{-1}. Furthermore, the sequential layer exchange allowed us to form a 2000-nm-thick SiGe layer. The output power density was almost proportional to t and reached

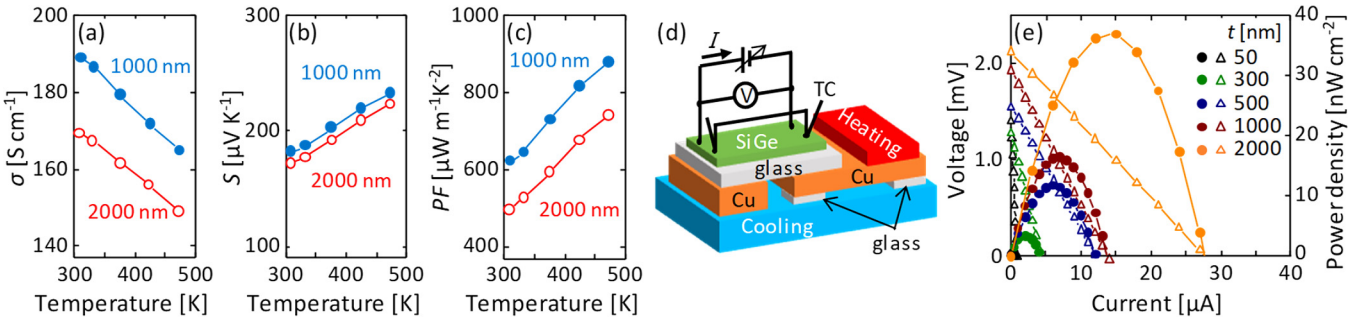

FIG. 6. (a) Electrical conductivity σ, (b) Seebeck coefficient S, and (c) power factor PF of the $Si_{0.4}Ge_{0.6}$ samples for $t = 1000$ and 2000 nm with respect to the measurement temperature. (d) Schematic of a system for the output power measurement. (e) Voltage–current (open triangles) and output power density (solid circles) for the SiGe samples with $t = 50$, 300, 500, 1000, and 2000 nm obtained under a constant temperature difference of 10 K and a sample stage temperature of 300 K.

37 nW cm^{-2} under a temperature difference of 10 K. Because ALILE-SiGe can be applied to plastic substrates, the findings in this study will present practical applications for human-friendly, flexible TEGs with high reliability.

ACKNOWLEDGMENTS

This study was financially supported by JST PRESTO (No. JPMJPR17R7) and the Thermal and Electric Energy Technology Foundation. The authors are grateful to Professor T. Sakurai (University of Tsukuba) for the Hall effect measurements and Ms. T. Tawara and Mr. K. Tanigawa (University of Tsukuba) for their help with experiments at the Nanotechnology Platform. The EBSD measurements were conducted at the International Center for Young Scientists in NIMS.

DATA AVAILABILITY

The data that support the findings of this study are available from the corresponding authors upon reasonable request.

REFERENCES

[1]I. Petsagkourakis, K. Tybrandt, X. Crispin, I. Ohkubo, N. Satoh, and T. Mori, Sci. Technol. Adv. Mater. **19**, 836 (2018).
[2]J.-H. Bahk, H. Fang, K. Yazawa, and A. Shakouri, J. Mater. Chem. C **3**, 10362 (2015).
[3]M. Bharti, A. Singh, S. Samanta, and D. K. Aswal, Prog. Mater. Sci. **93**, 270 (2018).
[4]Z. Lin, C. Hollar, J. S. Kang, A. Yin, Y. Wang, H. Y. Shiu, Y. Huang, Y. Hu, Y. Zhang, and X. Duan, Adv. Mater. **29**, 1606662 (2017).
[5]C. Yang, D. Souchay, M. Kneiß, M. Bogner, H. M. Wei, M. Lorenz, O. Oeckler, G. Benstetter, Y. Q. Fu, and M. Grundmann, Nat. Commun. **8**, 16076 (2017).
[6]J. Liang, T. Wang, P. Qiu, S. Yang, C. Ming, H. Chen, Q. Song, K. Zhao, T.-R. Wei, D. Ren, Y.-Y. Sun, X. Shi, J. He, and L. Chen, Energy Environ. Sci. **12**, 2983 (2019).
[7]B. Paul, E. M. Björk, A. Kumar, J. Lu, and P. Eklund, ACS Appl. Energy Mater. **1**, 2261 (2018).
[8]T. G. Novak, J. Kim, J. Kim, H. Shin, A. P. Tiwari, J. Y. Song, and S. Jeon, 2D Mater. **6**, 045019 (2019).
[9]J. P. Dismukes, L. Ekstrom, E. F. Steigmeier, I. Kudman, and D. S. Beers, J. Appl. Phys. **35**, 2899 (1964).
[10]C. B. Vining, J. Appl. Phys. **69**, 331 (1991).
[11]G. Joshi, H. Lee, Y. Lan, X. Wang, G. Zhu, D. Wang, R. W. Gould, D. C. Cuff, M. Y. Tang, M. S. Dresselhaus, G. Chen, and Z. Ren, Nano Lett. **8**, 4670 (2008).
[12]K. Xie, K. Mork, J. T. Held, K. Andre Mkhoyan, U. Kortshagen, and M. C. Gupta, J. Appl. Phys. **123**, 094301 (2018).
[13]K. Tajima, W. Shin, M. Nishibori, N. Murayama, T. Itoh, N. Izu, and I. Matsubara, Key Eng. Mater. **320**, 99 (2006).
[14]J. A. Perez-Taborda, M. Muñoz Rojo, J. Maiz, N. Neophytou, and M. Martin-Gonzalez, Sci. Rep. **6**, 32778 (2016).
[15]M. Takashiri, T. Borca-Tasciuc, A. Jacquot, K. Miyazaki, and G. Chen, J. Appl. Phys. **100**, 054315 (2006).
[16]Z. Wang, P. Fiorini, V. Leonov, and C. Hoof, J. Micromech. Microeng. **19**, 094011 (2009).
[17]R. Cheaito, J. C. Duda, T. E. Beechem, K. Hattar, J. F. Ihlefeld, D. L. Medlin, M. A. Rodriguez, M. J. Campion, E. S. Piekos, and P. E. Hopkins, Phys. Rev. Lett. **109**, 195901 (2012).
[18]J. Lu, R. Guo, W. Dai, and B. Huang, Nanoscale **7**, 7331 (2015).
[19]J. Lu, R. Guo, and B. Huang, Appl. Phys. Lett. **108**, 141903 (2016).
[20]A. Nozariasbmarz, A. Tahmasbi Rad, Z. Zamanipour, J. S. Krasinski, L. Tayebi, and D. Vashaee, Scr. Mater. **69**, 549 (2013).
[21]H. Takiguchi, M. Aono, and Y. Okamoto, Jpn. J. Appl. Phys. **50**, 041301 (2011).
[22]Y. Peng, L. Miao, J. Gao, C. Liu, M. Kurosawa, O. Nakatsuka, and S. Zaima, Sci. Rep. **9**, 14342 (2019).
[23]Z. Wang, L. P. H. Jeurgens, J. Y. Wang, and E. J. Mittemeijer, Adv. Eng. Mater. **11**, 131 (2009).
[24]K. Toko and T. Suemasu, J. Phys. D Appl. Phys. **53**, 373002 (2020).
[25]K. Kusano, A. Yamamoto, M. Nakata, T. Suemasu, and K. Toko, ACS Appl. Energy Mater. **1**, 5280 (2018).
[26]M. Tsuji, K. Kusano, T. Suemasu, and K. Toko, Appl. Phys. Lett. **116**, 182105 (2020).
[27]M. Tsuji, T. Imajo, N. Saitoh, N. Yoshizawa, T. Suemasu, and K. Toko, J. Phys. D Appl. Phys. **53**, 075105 (2020).
[28]P. M. Mooney, F. H. Dacol, J. C. Tsang, and J. O. Chu, Appl. Phys. Lett. **62**, 2069 (1993).
[29]Y. Nakamura, M. Isogawa, T. Ueda, S. Yamasaka, H. Matsui, J. Kikkawa, S. Ikeuchi, T. Oyake, T. Hori, J. Shiomi, and A. Sakai, Nano Energy **12**, 845 (2015).
[30]J. Y. W. Seto, J. Appl. Phys. **46**, 5247 (1975).
[31]T. Imajo, K. Moto, R. Yoshimine, T. Suemasu, and K. Toko, Appl. Phys. Express **12**, 015508 (2019).
[32]F. A. Trumbore, Bell Syst. Tech. J. **39**, 205 (1960).
[33]S.-Y. Wei, S.-M. Yu, H.-H. Lin, W. Chen, C.-J. Chen, T.-S. Lin, C.-H. Tsai, and F.-R. Chen, in *2010 35th IEEE Photovoltaic Specialists Conference* (IEEE, 2010), pp. 001586–001588.